

Molecular Weight Dependence of Polymersome Membrane Structure, Elasticity, and Stability

Harry Bermudez*, Aaron K. Brannan[†],
Daniel A. Hammer*, Frank S. Bates[†], and Dennis E. Discher*,[‡]

[†]*School of Engineering and Applied Science, University of Pennsylvania, Philadelphia PA 19104,*

[‡]*Department of Chemical Engineering and Materials Science, University of Minnesota, Minneapolis
MN 55455*

Classification: Physical Sciences - Applied Physical Sciences

Manuscript Information: 18 pages

Word and character counts: 195 words in abstract and 38,958 characters in paper

[‡]To whom correspondence should be addressed: School of Engineering and Applied Science, 112 Towne Bldg., University of Pennsylvania, Philadelphia PA 19104. Phone: 215-898-4809, Fax: 215-573-6334, E-mail: discher@seas.upenn.edu

Abstract

Vesicles prepared in water from a series of diblock copolymers - “polymer-somes” - are physically characterized and compared to lipid vesicles. With increasing molecular weight \bar{M}_n , the hydrophobic core thickness d for the self-assembled bilayers of poly(ethylene oxide)-polybutadiene (PEO-PBD) increases up to $\simeq 20$ nm - considerably greater than any previously studied lipid system. The mechanical responses of these membranes, specifically, the area elastic modulus K_a and maximal areal strain α_c are measured by micromanipulation. As expected for interface-dominated elasticity, K_a ($\simeq 100$ pN/nm) is found to be independent of \bar{M}_n , but lower than the usual values for zwitterionic lipid membranes. Experiments on polymer-somes show α_c increases in a nearly linear fashion with \bar{M}_n , approaching a limiting value predicted by mean-field ideas which is universal and about 10-fold above that typical of lipids. Nonlinear responses and memory effects generally emerge with increasing \bar{M}_n , indicating the onset of chain entanglements at higher \bar{M}_n . The effects of \bar{M}_n thus suggest a compromise between stability and fluidity for biomembranes. More generally, the results highlight the interfacial limits of self-assemblies at the nanoscale.

Biological systems of all sorts have long been appreciated as exploiting aqueous self-assembly; synthetic amphiphiles of many types have also been shown to spontaneously self-assemble into highly ordered structures in water [1–6]. Depending on temperature and molecular characteristics such as geometry, numerous morphologies are now possible, including vesicles, micelles, and more exotic structures. Even so, the factors contributing to microphase stability are not always clear at the nanoscale, where interfacial effects often dominate bulk interactions. Towards addressing these issues we describe the material properties of vesicle membranes made from a novel molecular weight series of diblock copolymers.

Lipid vesicles or “liposomes” [7] are often considered the prototypical membrane systems. As such, they have received considerable attention that has proven relevant to the fundamentals of membrane behavior and to the motivation for biomimics [8]. However, practical applications involving liposomes have been continually hindered by a lack of stability [9]. Presumably commensurate with limits on membrane stability is the narrow range (3–5 nm) of the hydrophobic core thickness d of liposome membranes [10]. We are able to extend the range of d and explore the impact on membrane properties by forming vesicles from diblock copolymers of poly(ethylene oxide)-polybutadiene (PEO-PBD) [11].

[TABLE 1 about here.]

Materials and Methods

Materials As listed in Table I, a novel molecular weight series of PEO-PBD as well as PEO-poly(ethylene) was synthesized by standard living anionic polymerization techniques [12]. The number of monomer units in each block was determined by $^1\text{H-NMR}$. Gel-permeation chromatography with polystyrene standards was used to determine number-average molecular weights \bar{M}_n as well as polydispersity indices (always < 1.10). The PEO volume fraction is denoted by f_{EO} . For comparison, the phospholipids SOPC (1-stearoyl-2-oleoyl phosphatidylcholine) and DMPC (1,2-dimyristoyl phosphatidylcholine) have hydrophilic volume fractions $f \simeq 0.30$ and 0.36 , respectively.

Preparation of Polymer Vesicles Giant vesicles were made by film rehydration. Briefly, 10 – 50 μL of a 4 mg/mL copolymer in chloroform solution was uniformly coated on the inside wall of a glass vial, followed by evaporation of the chloroform under vacuum for 3 h. Addition of sucrose solution (250 – 300 mM) led to spontaneous budding of vesicles off of the glass and into solution. Copolymers of higher molecular weight (*i.e.*, **OB18**, **OB19**) required incubation at $\simeq 60^\circ\text{C}$ to increase vesicle size and yield. Vesicles were usually suspended in phosphate-buffered saline (PBS).

Cryogenic Transmission Electron Microscopy (cryo-TEM) Thin films (about 10-300 nm) of 1.0 wt% polymer in water were suspended in a microperforated grid. Samples were prepared in an isolated chamber with temperature and humidity control. The sample assembly was rapidly vitrified with liquid ethane at its melting temperature ($\simeq 90\text{ K}$), and kept under liquid nitrogen until it was loaded onto a cryogenic sample holder (Gatan 626). Images were obtained with a JEOL 1210 at 120 kV using a nominal underfocus of 6 μm for improved phase contrast and digital recording. For a more detailed description and related examples,

see [13,14].

Optical Microscopy and Micromanipulation A Nikon TE-300 inverted microscope with Narishige manipulators was used for micropipette manipulation of vesicles. A custom manometer system with pressure transducers (Validyne, Northridge, CA) allowed for control and monitoring of the pressure. Imaging was done with either a 40 \times , 0.75 NA air objective lens under bright-field illumination or a 20 \times , 0.5 NA phase objective lens for phase contrast imaging. Bright-field imaging was used for clear visualization of the vesicle membrane, whereas phase contrast was used when a difference in refractive indices was established between the interior and exterior solutions (*e.g.*, sucrose inside and PBS outside). The contrast is visibly moderated by any exchange of solutes across the membrane.

Mechanical properties of polymersome membranes were measured by micropipette aspiration methods. As described previously [6,15,16], a giant vesicle aspirated into a micropipette (of internal radius R_p) under an applied pressure ΔP leads to a projection length of membrane ΔL . These two measured quantities are used to calculate the imposed membrane tension τ and the relative area dilation $\alpha \equiv \Delta A/A_o$ from the Law of Laplace and the outer vesicle radius R_v :

$$\tau = \frac{1}{2} \frac{\Delta P R_v R_p}{(R_v - R_p)}$$

$$\Delta A \simeq 2\pi R_p \Delta L \left(1 - \frac{R_p}{R_v}\right)$$

The quantities τ and α are the 2-dimensional analogues of bulk stress and strain. Measurements on 10 – 20 individual vesicles are used to determine the average (\pm S.D.) properties of membranes reported below.

Results and Discussion

Among all of the various vesicle-forming amphiphiles, including lipids, a key unifying feature is a hydrophilic fraction $f \simeq 0.3 - 0.4$ (Table I). Aqueous self-assembly of the present diblocks into membranes requires such proportions, as it is well-documented theoretically [17] and experimentally [18] that a larger f leads to wormlike and spherical micelles while smaller values of f yield inverted phases. Another shared feature of lipid membranes is their narrow range of hydrophobic core thickness d of 3 – 5 nm. Connections between molecular conformations and mass, as well as the interplay between these factors in determining and limiting membrane self-assembly, thus have not been thoroughly studied. Our novel series of PEO-PBD diblock copolymers allows us to extend the narrow range of d for vesicles. Direct imaging of vesicles by cryo-TEM demonstrates a systematic increase in d with \bar{M}_n (Table I and Fig. 1).

[FIG. 1 about here.]

It is important to note that the depth-of-field for cryo-TEM is comparable to the sample film thickness used. As such, the resulting image is effectively the projection of a sample’s density into a plane. Assuming a membrane core of homogeneous density and spherical

vesicles, the projected density leads to a maximum in the intensity I at the vesicle inner radius $r = R_i$. At $r = R_i + d$, the intensity will go to zero, or in our case, to the background intensity I_o . This simple model for the intensity is shown in Figure 2a, where d/R_i is used as a free parameter. For $d/R_i < 0.25$, the model is in excellent agreement with the measured profile (circumferentially-averaged). The dark and light rings seen in Figure 1 are Fresnel interference fringes corresponding to the abrupt changes in projected density at the inner and outer edges of the membrane, respectively. The fringes can also be seen in Figure 2a at $r \simeq R_i$ and $r \simeq R_i + d$, thus providing a simple means for determining the membrane thickness d . Similar analysis of spherical micelles via cryo-TEM gives very comparable results to corresponding SANS measurements [11,18].

[FIG. 2 about here.]

Measurements of d are shown in Figure 2b, based on either fitting experimental profiles, or otherwise, edge detection. The results seem to be independent of vesicle radius even though contrast is reduced for smaller vesicles. For all vesicle systems, d has a standard deviation of $\pm 1 - 1.5$ nm.

Glassy diblock copolymers of PEO-polystyrene and poly(acrylic acid)-polystyrene have previously been shown to generate vesicular shells in organic mixtures with added water [19] but no clear relationship between copolymer molecular weight and membrane thickness has yet been described. The thickness measurements here for our self-assembling copolymers suggest a scaling relationship between d and \bar{M}_n . Noting that the mean hydrophobic molecular weight is given by $\bar{M}_h \simeq \bar{M}_n(1 - f)$, the experimental scaling of $d \sim (\bar{M}_h)^a$ leads to an exponent $a \simeq 0.60$ (Fig. 3). The exponent a is minimally affected by including lipid data, yet considerably expands the range of \bar{M}_h . Regardless, this scaling result can offer insight into the chain conformations within the membrane core. In theory, fully stretched chains would give $a = 1$ and random coils would give $a = 1/2$. Our copolymers are expected to be in the strong segregation limit (SSL), where a balance of interfacial tension and chain entropy yield a scaling of $a = 2/3$ [17]. The best-fit scaling exponent therefore suggests that chains in the various polymersome membrane cores are stretched to some extent.

[FIG. 3 about here.]

Compared to non-equilibrated membranes of PEO-polystyrene, **OE7** and **OB18** membranes have been clearly shown to be fluid via in-plane mobility measurements, although lateral diffusivity decreases strongly with \bar{M}_n [20]. Fluidity generally allows for an equilibration of net forces that underlie the scaling exponent a above, but there is also evidence for partial collapse of the PEO chains towards the interface, thus shielding the hydrophobic core from water [18]. This collapse would have the effect of increasing the equilibrium area per chain \mathcal{A} and decreasing membrane thickness, consistent with a slightly smaller exponent a compared to the SSL. Assuming incompressibility, one can show that $\mathcal{A} \sim (\bar{M}_h)^{0.4}$. Additional effects associated with relatively low \bar{M}_n polymers may also play a role in the scaling behavior.

The high edge-contrast seen from the cryo-TEM images (Fig. 1) further suggests that the interface between the hydrophobic core and the PEO corona is fairly narrow for all of the polymersomes. This is consistent with theoretical predictions for copolymers in the SSL

since interfacial thickness should scale with the Flory interaction parameter χ as $\sim \chi^{-0.5}$ but not with \bar{M}_n [21]. This qualitative observation on interfacial thickness is a first clue that the interfacial tension γ driving the self-assembly of the diblocks in water is essentially constant for this series.

Determinations of membrane elasticity and strength lend deeper insight into the interfacial and bulk forces at work within polymersome membranes. These forces have been probed by micropipette aspiration techniques (Fig. 4) pioneered by Evans and coworkers [15] with giant unilamellar lipid vesicles. Plots of the effective membrane tension τ against the mean dilational strain α reveal an initial linear response as well as subsequent nonlinear and hysteretic effects. The latter are obvious for the thicker membranes **OB18** and **OB19** at areal strains ($>10\text{-}20\%$) much greater than those sustainable by any lipid membrane. Nonlinear behavior and hysteresis are thus not accessible with any of the various elastic lipid systems. Nevertheless, the reproducible initial slope of τ versus α defines an area elastic modulus K_a for the membrane (Fig. 4).

[FIG. 4 about here.]

Only one series of single component phospholipid membranes (consisting of saturated and unsaturated phosphatidylcholines) has been thoroughly characterized. The most recent and refined measurements give $K_a \simeq 240$ pN/nm [16]. The considerable thermal undulations of lipid membranes complicate K_a measurements, requiring a significant correction to account for the entropic contributions to area dilation. For our polymersomes this effect is mitigated by membranes that are the substantially thicker, and hence stiffer out-of-plane; for **OE7**, the correction to α is only about 1%.

In addition to hydrophobic interactions, other factors affecting K_a can arise from the counterion pairing expected among zwitterionic amphiphiles or the presence of small molecules, such as cholesterol, in the membrane. These complexities are avoided by the use of single-component, neutral systems such as those here. Hence we can essentially view K_a as being primarily related to the interfacial tension γ that reflects the chemical composition at each interface of the membrane. A simple area elasticity calculation [22] based on balancing molecular compression ($\sim 1/\mathcal{A}$) against interfacial energy ($\sim \mathcal{A}\gamma$) gives $K_a = 4\gamma$.

[FIG. 5 about here.]

The chemical rather than physical basis for γ leads one to expect that K_a is independent of \bar{M}_n (and hence d). Indeed a mean K_a of 102 ± 10 pN/nm is obtained for all of the various polymersomes (Fig. 5). This includes **OE7**, which is simply a hydrogenated **OB**. Surface elasticity of the membrane thus depends *only* on the interface. Moreover, enthalpic interactions between PEO chains, which have been speculated to include H₂O bridging [23] or crystallization [12] are either independent of PEO length or simply not a factor. A value of $\gamma = K_a/4 = 26$ pN/nm is also very typical of oil-water interfaces. As mentioned, γ and χ are related and provide a measure of segregation between blocks; specifically, $\gamma \sim \sqrt{\chi}$ [21]. The results thus suggest that a combined knowledge of amphiphile geometry (*i.e.*, f) and interaction energies (χ) lead to predictive insights into membrane structure and elasticity.

While phosphatidylcholine membranes appear slightly stiffer than the present polymersome membranes, no lipid membrane can be strained by more than a critical strain $\alpha_c \simeq 5\%$

before rupture, regardless of cholesterol addition. In contrast, the present synthetic systems can be strained to almost 50%, with a nearly linear dependence on molecular weight (Fig. 6). At such large strains, an incompressible membrane will thin considerably to a reduced thickness $d_c \equiv d/(1 + \alpha_c)$. Using the previous relation $d \sim (\bar{M}_h)^a$ gives the scaling $\alpha_c \sim d_c^b$ with $b \simeq 1.7$. This scaling excludes the largest copolymer, **OB19**, which generally exhibits the earliest onset of hysteresis and falls well below the trend (Fig. 6). As explained below, the apparent τ_c and α_c are both smaller for **OB19** ($\tau_c = 22 \pm 5$ pN/nm) than for **OB18** ($\tau_c = 33 \pm 5$ pN/nm). Thus, although larger copolymers allow for larger areas per chain \mathcal{A} , there are upper bounds on the strain (and stress) that can be withstood by a membrane.

[FIG. 6 about here.]

The same balance of forces used to understand the SSL and membrane elasticity provides insight into membrane stability limits. The net chain pressure Π (core plus headgroup) and applied tension τ are balanced by the interfacial tension γ :

$$\Pi + \tau = 2\gamma \quad (1)$$

To account for the nonlinearity in the aspiration plots of Figure 4, the isotropic membrane tension is expanded [15] to second order:

$$\tau(\alpha) = \tau_0 + K_a\alpha + \frac{1}{2} \frac{\partial^3 F}{\partial \alpha^3} \alpha^2 \quad (2)$$

Because of isotonic conditions, $\tau_0 = 0$, and the experiments are well-fit by

$$\tau(\alpha) = K_a(\alpha - c\alpha^2) \quad (3)$$

with the coefficient $c \equiv -K_a^{-1}(\frac{1}{2}\partial^3 F/\partial \alpha^3)$ having the average value of 1.0 ± 0.2 for **OB9**, **OB18** and **OB19**. Using the previously cited mean-field result of $K_a = 4\gamma$, we obtain

$$\Pi + K_a(\alpha - \alpha^2) = \frac{1}{2}K_a \quad (4)$$

and solve for α to arrive at

$$\alpha = \frac{1}{2} \left(1 \pm \sqrt{\Pi/\gamma - 1} \right) \quad (5)$$

From Eq. (5), there can only be real solutions provided that $\Pi \geq \gamma$. Noting that $\Pi = 2\gamma$ at zero applied tension, $\gamma \leq \Pi \leq 2\gamma$. Establishing the bounds for Π allows us to do the same for τ via Eq. (1) such that $\gamma \geq \tau \geq 0$. The upper bound for τ could also have been obtained by setting $d\tau/d\alpha = 0$ from Eq. (3).

By definition, $\alpha \geq 0$, but solutions of Eq. (5) with the positive root give $\frac{1}{2} \leq \alpha \leq 1$ whereas those with the negative root give $0 \leq \alpha \leq \frac{1}{2}$. Only the latter makes physical sense, corresponding to $\Pi/\gamma = 1 - 2$ and $\tau/\gamma = 1 - 0$. The above bounds of $\alpha \leq \frac{1}{2}$ and $\tau \leq \gamma$ largely agree with the experimentally observed limits self-assembled polymersome membranes. A related case where the core polymer is treated as a three-dimensional brush [16] would give $\alpha \leq 0.21$, which is exceeded here. The overall membrane behavior also

appears rather insensitive to any local variations associated with finite polydispersity and seems instead dominated by the collective behavior of a fluid or melt-like state. Thus the increased thickness (*i.e.*, larger \bar{M}_n) makes the interface more readily self-healing. In natural membranes, by comparison, stiffening and toughening of the membranes is mediated by the small molecule cholesterol - presumably through cohesive healing of defects. However, the additional stability imparted by cholesterol to biomembranes cannot compare with that of a much thicker membrane. The results here therefore imply that biomembranes are not designed for maximal stability, but are instead optimized for a balance between stability and fluidity.

The nonlinearity seen in the stress-strain curves, $\tau(\alpha)$, also appears distinctive and revealing. As already noted, lipid membranes cannot withstand areal strains exceeding $\simeq 5\%$ and therefore a strictly linear elastic response is not surprising. For such systems, the corresponding first-order analysis ($c = 0$) of the stability limit again yields $\alpha \leq \frac{1}{2}$ (independent of γ), although the additional conditions of $\Pi/\gamma \geq 1$ and $\tau/\gamma \leq 1$ would not be apparent. The basis for the strain-softening seen here is not clear. The nonlinearity is not strongly dependent on deformation rate, suggesting that this is not a collective process involving many molecules but is instead a rearrangement at the molecular scale. We speculate that area dilation decreases PEO stretching and allows more collapse and hence shielding of the hydrophobic core. The proposed process is inspired in part by compressed monolayers which tend to show a decreased slope in their pressure isotherms during large dilations.

The decreased stability of the thickest membrane (**OB19**) is also unclear at this point but seems likely to be the result of increasing physical entanglements between chains. The inset to Figure 4b is representative of the very slow relaxation dynamics of **OB19** membranes. Even in **OB18**, membrane dynamics following electroporation are more than 100 times slower than **OE7** dynamics [25]. Furthermore, lateral diffusion coefficients beginning with **OB18** exhibit activated reptation [20], which is a much stronger function of \bar{M}_n than simple Rouse diffusion.

Provided that the timescale for aspiration is much smaller than the timescale for rearrangement among polymer chains (as is likely at the largest \bar{M}_n), the entanglements present could act in a similar way to covalent crosslinks. Surprising perhaps, but consistent with the results here, polymersome membranes with very low crosslink densities have been found to be weaker than uncrosslinked membranes [26]. This destabilization presumably arises through stress localization; that is, the tension τ is inhomogeneous over the membrane due to slow relaxations that oppose equilibration of forces.

Non-equilibrium effects indicated above can also be seen in τ - α hysteresis loops following graded release from aspiration (Fig. 4). Even down to low apparent areal strains of less than 10%, **OB19** exhibits marked hysteresis, whereas **OB18** aspiration appears reversible up to more modest strains of $\simeq 10 - 15\%$. In contrast, aspiration of **OE7** is reversible for nearly all strains up to lysis [6], consistent with diffusion studies indicating Rouse-type mobility [20]. Hence the hysteretic behavior in thicker membranes likely reflects relaxation times that scale strongly [28] with \bar{M}_n .

Conclusions

Vesicles formed by superamphiphiles provide new insight into some of the basic properties of bilayer membranes. By use of synthetic diblock copolymers, limitations of previous

membrane systems have been considerably exceeded, providing novel insights into structure, scaling and physical limits on lamellae. Specifically, the surface elasticity is found to be scale-independent, in accordance with simple mean-field theories. The membrane lysis tension τ_c and critical areal strain α_c are found to increase with \bar{M}_n , but only up to a simple limit. The onset of chain entanglements with higher \bar{M}_n introduces novel bulk effects that eventually undermine interfacial elasticity through slowed response times. Examination of membranes assembled from PEO-PBD-PEO triblocks, where linear and looped configurations are expected, may help clarify such mechanisms. Of additional interest will be determinations of other properties such as the bending modulus which is expected to scale as $\sim K_a d^2$ [6] for interface-dominated membranes. Finally, while it is clear that lipid membranes found in nature are not maximally stable, they have developed sufficient stability while also providing the fluidity necessary for diverse functions.

This work was supported by NSF-MRSEC's at Penn and University of Minnesota as well as a materials science grant from NASA. HB thanks Dr. H. Aranda-Espinoza at Penn for many valuable conversations. The authors also acknowledge useful discussions with Prof. E.A. Evans at Boston University.

REFERENCES

- [1] Cornelissen, J.J.L.M., Fischer, M., Sommerdijk, N.A.J.M., and Nolte, R.J.M. (1998) *Science* **280** 1427-1430.
- [2] van Hest, J.C.M., DeInoye, D.A.P., Baars, M.W.P.L., van Genderen, M.H.P., and Meijer, E.W. (1995) *Science* **268** 1592-1595.
- [3] Kramer, E., Forster, S., Goltner, C., and Antonietti, M. (1998) *Langmuir* **14** 2027-2031.
- [4] Nardin, C. Hirt, T., Leukel, J., and Meier, W. (2000) *Langmuir* **16** 1035-1041.
- [5] Kaler, E.W., Murthy A.K., Rodriguez B.E., and Zasadzinski J.A.N. (1989) *Science* **245** 1371-1374.
- [6] Discher, B.M., Won, Y-Y., Ege, D.S., Lee, J.C-M., Bates, F.S., Discher, D.E., and Hammer, D.A. (1999) *Science* **284**, 1143-1146.
- [7] Bangham, A.D., Standish, M.M., and Watkins, J.C. (1967) *J. Mol. Biol.* **13**, 238-252.
- [8] Lipowsky, R. and Sackmann, E. (1995) in *Structure and Dynamics of Membranes* (Elsevier, New York).
- [9] Lasic, D.D. and Papahadjopoulos, D. (1998) in *Medical applications of liposomes* (Elsevier, New York).
- [10] Marsh, D. (1990) in *CRC Handbook of lipid bilayers* (CRC Press, Boca Raton, FL).
- [11] Won, Y-Y., Davis, H.T., and Bates, F.S. (1999) *Science* **283**, 960-963.
- [12] Hillmyer, M.A., and Bates, F.S. (1996) *Macromolecules* **29**, 6994-7002.
- [13] Lin, Z., He, M., Scriven, L.E., and Davis, H.T. (1993) *J. Phys. Chem.* **97**, 3571-3578
- [14] Vinson, P.K., Talmon, Y., and Walter, A. (1989) *Biophys. J.* **56**, 669-681.
- [15] Evans, E.A. and Skalak, R. (1980) in *Mechanics and Thermodynamics of Biomembranes* (CRC Press, Boca Raton, FL).
- [16] Rawicz, W., Olbrich, K.C., McIntosh, T., Needham, D., Evans, E. (2000) *Biophys. J.* **79**, 328-339.
- [17] Bates, F.S., and Fredrickson, G.H. (1990) *Annu. Rev. Phys. Chem.* **41**, 525-557.; Bates, F.S. (1991) *Science* **251**, 898-905.
- [18] Won, Y-Y., Davis, H.T., Bates, F.S., Agamalian, M., and Wignall, G.D. (2000) *J. Phys. Chem. B* **104**, 7134-7143.
- [19] Yu, K. and A. Eisenberg (1998) *Macromolecules* **31**, 3509-3518.; Yu, Y., Zhang, L. and A. Eisenberg (1998) *Macromolecules* **31**, 1144-1154.
- [20] Lee, J.C-M., Santore, M.M., Bates, F.S., and Discher, D.E. (2002) *Macromolecules* **35**, 323-326.
- [21] Helfand, E. and Wasserman, Z.R. (1982) in *Developments in Block Copolymers, vol. I*, ed. Goodman, I. (Applied Science, New York), p. 99-125.
- [22] Israelachvili, J.N. (1998) in *Intermolecular and Surface Forces* (Academic Press, Inc. San Diego, CA).
- [23] Naumann, C.A., Brooks, C.F., Fuller, G.G., Lehmann, T., Ruhe, J., Knoll, W., Kuhn, P., Nuyken, O., and Frank, C.W. (2001) *Langmuir* **17**, 2801-2806.
- [24] Ferry, J.D. (1980) in *Viscoelastic Properties of Polymers* (Wiley, New York).
- [25] Aranda-Espinoza, H., Bermudez, H., Bates, F.S., and Discher, D.E. (2001) *Phys. Rev. Lett.* **87**, 208301.
- [26] Discher, B.M., Bermudez, H., Hammer, D.A., Discher, D.E., Won, Y-Y., and Bates, F.S. (*in press*).
- [27] Evans, E., and Ludwig, F. (2000) *J. Phys.* **12**, A315-320.

- [28] Hamersky, M.W., Hillmyer, M.A., Tirrell, M., Bates, F.S., Lodge, T.P., and von Meerwall, E.D. (1998) *Macromolecules* **31**, 5363-5370.

List of Figures

- 1 Cyro-TEM images of a 1.0 wt% aqueous solution of copolymer in water: (a) **OB2**, (b) **OB18**, and (c) **OB19**. The hydrophobic cores of polybutadiene are the darker areas. Scale bars are 100 nm. Polymorphism is common in cryo-TEM preparations [6] but does not pose any difficulties to analysis since vesicles can be clearly identified from their concentric-ring structure. 14
- 2 (a) Experimental intensity profile of a vesicle imaged by cryo-TEM. Best fit of the data corresponds to $d/R_i = 0.25$, *cf.* experimental measurement of $d/R_i = 0.27$; a difference of less than 1 nm. Dash-dot and dashed lines indicate fits using $d/R_i = 0.2$ and 0.3 , respectively. Note the Fresnel interference fringe at $r/R_i \approx 1.3$. (b) Dependence of measured hydrophobic thickness d on inner radius R_i of vesicles imaged by cryo-TEM for **OB2**, **OB18** and **OB19**. Solid and dashed lines are mean values \pm S.D. Data are shown using spherical vesicles (\circ) and out-of-plane curvature estimates (Δ) for nonspherical vesicles. 15
- 3 Scaling of core thickness d with hydrophobic molecular weight \bar{M}_h . The best-fit scaling exponent of 0.6 is suggestive of chains stretching relative to their unperturbed state but exponents of $1/2$ and $2/3$ (solid grey and dashed grey, respectively) also fit the data reasonably well. Data are shown for membranes of various phospholipids (Δ) [10], **OE7** (\circ), and the **OB** series (\square). 16
- 4 Determination of mechanical properties by micropipette aspiration. The applied tension τ is plotted against areal strain α and the area elastic modulus K_a is determined from the initial slope. Unlike **OE7** vesicles whose aspiration is entirely reversible [6], hysteresis is observed after large strains imposed upon **OB18** and **OB19** vesicles. (a) **OB18** vesicle aspiration (\bullet) and subsequent release (\circ). The inset shows a typical aspiration process in bright-field imaging. (b) **OB19** membranes do not relax quickly to their original state. The inset shows the slow dynamics of a twice-aspirated **OB19** vesicle under phase contrast. In all experiments the loading rate ranged from $\simeq 1 - 10 \times 10^{-4} \text{Nm}^{-1}\text{sec}^{-1}$, without significant effect on the reported properties. Scale bars are $5 \mu\text{m}$ 17
- 5 Molecular weight independence of the area elastic modulus K_a . The dominant factor in determining K_a is the interfacial tension γ or equivalently, the interaction parameter χ that drives segregation. The membrane elasticity is thus determined strictly by the chemical composition of the interface and not the size of the molecule. Membranes of phosphatidylcholines (PC) have somewhat higher values of K_a [16], reflecting the distinct composition. Data are shown for various PC (Δ) [16], **OE7** (\circ), and **OB** (\square) vesicles. Mean K_a is $102 \pm 10 \text{ pN/nm}$ 18

- 6 Areal strain at rupture α_c versus hydrophobic molecular weight. Scaling behavior is almost that of a simple linear dependence with an exponent $\simeq 0.94$. Data are shown for SOPC (\triangle), **OE7** (\circ), and **OB** (\square) vesicles. The predicted upper limit of 50% is universal to bilayer systems. Note that lipid membranes are well below this bound and typically do not exceed $\simeq 5\%$ areal strains. The hatched region schematically illustrates the molecular weight range where chain entanglements are thought to contribute [24]. 19

FIGURES

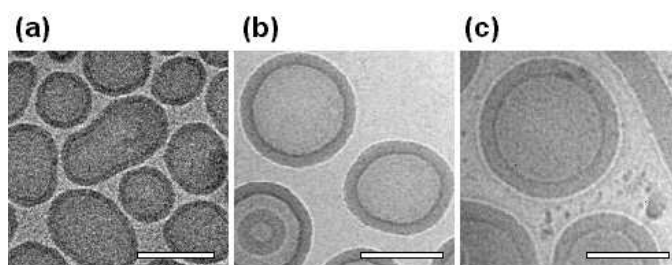


FIG. 1. Cryo-TEM images of a 1.0 wt% aqueous solution of copolymer in water: (a) **OB2**, (b) **OB18**, and (c) **OB19**. The hydrophobic cores of polybutadiene are the darker areas. Scale bars are 100 nm. Polymorphism is common in cryo-TEM preparations [6] but does not pose any difficulties to analysis since vesicles can be clearly identified from their concentric-ring structure.

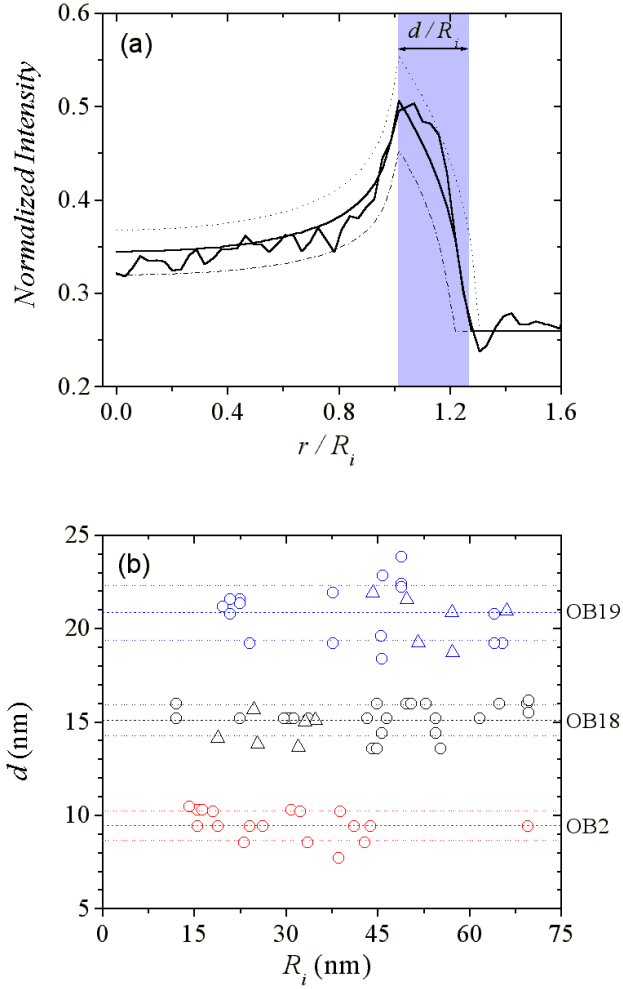


FIG. 2. (a) Experimental intensity profile of a vesicle imaged by cryo-TEM. Best fit of the data corresponds to $d/R_i = 0.25$, *cf.* experimental measurement of $d/R_i = 0.27$; a difference of less than 1 nm. Dash-dot and dashed lines indicate fits using $d/R_i = 0.2$ and 0.3 , respectively. Note the Fresnel interference fringe at $r/R_i \approx 1.3$. (b) Dependence of measured hydrophobic thickness d on inner radius R_i of vesicles imaged by cryo-TEM for **OB2**, **OB18** and **OB19**. Solid and dashed lines are mean values \pm S.D. Data are shown using spherical vesicles (\circ) and out-of-plane curvature estimates (\triangle) for nonspherical vesicles.

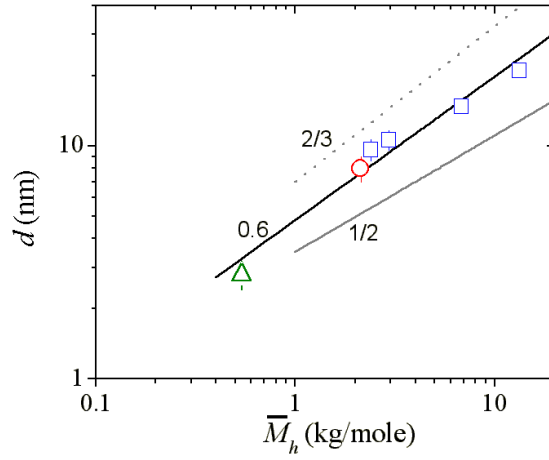


FIG. 3. Scaling of core thickness d with hydrophobic molecular weight \bar{M}_h . The best-fit scaling exponent of 0.6 is suggestive of chains stretching relative to their unperturbed state but exponents of 1/2 and 2/3 (solid grey and dashed grey, respectively) also fit the data reasonably well. Data are shown for membranes of various phospholipids (Δ) [10], **OE7** (\circ), and the **OB** series (\square).

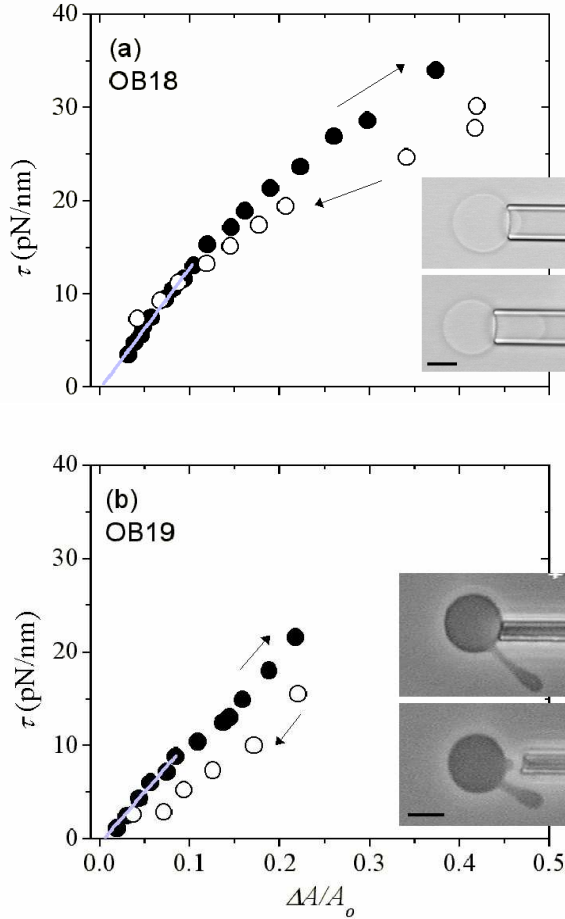


FIG. 4. Determination of mechanical properties by micropipette aspiration. The applied tension τ is plotted against areal strain α and the area elastic modulus K_a is determined from the initial slope. Unlike **OE7** vesicles whose aspiration is entirely reversible [6], hysteresis is observed after large strains imposed upon **OB18** and **OB19** vesicles. (a) **OB18** vesicle aspiration (\bullet) and subsequent release (\circ). The inset shows a typical aspiration process in bright-field imaging. (b) **OB19** membranes do not relax quickly to their original state. The inset shows the slow dynamics of a twice-aspirated **OB19** vesicle under phase contrast. In all experiments the loading rate ranged from $\simeq 1 - 10 \times 10^{-4} \text{Nm}^{-1}\text{sec}^{-1}$, without significant effect on the reported properties. Scale bars are 5 μm .

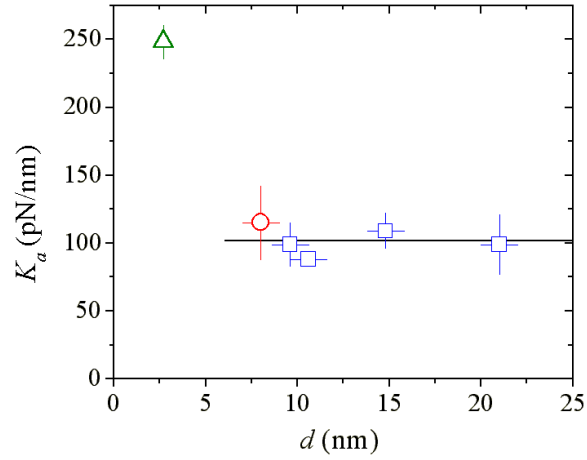


FIG. 5. Molecular weight independence of the area elastic modulus K_a . The dominant factor in determining K_a is the interfacial tension γ or equivalently, the interaction parameter χ that drives segregation. The membrane elasticity is thus determined strictly by the chemical composition of the interface and not the size of the molecule. Membranes of phosphatidylcholines (PC) have somewhat higher values of K_a [16], reflecting the distinct composition. Data are shown for various PC (Δ) [16], **OE7** (\circ), and **OB** (\square) vesicles. Mean K_a is 102 ± 10 pN/nm.

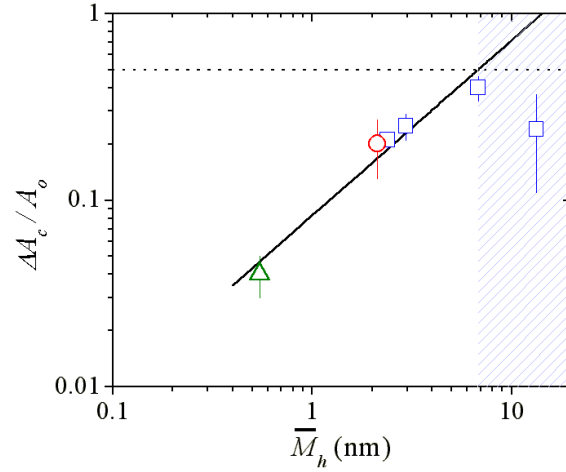


FIG. 6. Areal strain at rupture α_c versus hydrophobic molecular weight. Scaling behavior is almost that of a simple linear dependence with an exponent $\simeq 0.94$. Data are shown for SOPC (Δ), **OE7** (\circ), and **OB** (\square) vesicles. The predicted upper limit of 50% is universal to bilayer systems. Note that lipid membranes are well below this bound and typically do not exceed $\simeq 5\%$ areal strains. The hatched region schematically illustrates the molecular weight range where chain entanglements are thought to contribute [24].

List of Tables

I	Diblock copolymers and membrane core thickness d examined here.	21
---	---	----

TABLES

TABLE I. Diblock copolymers and membrane core thickness d examined here.

Designated Name	Polymer Formula	\bar{M}_n (kg/mol)	f_{EO}	d (nm)
OE7	EO ₄₀ -EE ₃₇	3.9	0.39	8.0±1
OB2	EO ₂₆ -BD ₄₆	3.6	0.28	9.6±1
OB9	EO ₅₀ -BD ₅₅	5.2	0.37	10.6±1
OB18	EO ₈₀ -BD ₁₂₅	10.4	0.29	14.8±1
OB19	EO ₁₅₀ -BD ₂₅₀	20.0	0.28	21.0±1